

A Performance-Based Wind Engineering Framework for Engineered Building Systems subject to Hurricanes

Zhicheng Ouyang ¹ and Seymour M.J. Spence ^{1,*}

¹ Department of Civil Engineering, University of Michigan, Ann Arbor, MI 48109, United States

Correspondence*: Corresponding Author smjs@umich.edu

2 ABSTRACT

- 3 Over the past decade, significant research efforts have been dedicated to the development of performance-based wind engineering (PBWE). Notwithstanding these efforts, frameworks 4 that integrate the damage assessment of the structural and envelope system are still lacking. 5 In response to this need, the authors have recently proposed a PBWE framework that holisti-6 7 cally treats envelope and structural damages through progressive multi-demand fragility models that capture the inherent coupling in the demands and damages. Similarly to other PBWE methodologies, this framework is based on describing the hurricane hazard through a nomi-9 nal straight and stationary wind event with constant rainfall and 1-hour duration. This paper aims 10 to develop a PBWE framework based on a full description of the hurricane hazard in which 11 the entire evolution of the storm track and time-dependent wind/rain fields is simulated. Hurri-12 cane induced pressures impacting the building envelope are captured through the introduction of a non-stationary/-straight/-Gaussian wind pressure model. Time-dependent wind-driven rain is modeled through a computational fluid dynamics Eulerian multiphase framework with interpo-15 lation schemes for the rapid computation of wind-driven rain intensities over the building surface. Through the development of a conditional stochastic simulation algorithm, envelope performa-17 nce is efficiently characterized through probabilistic metrics associated with rare events of design 18 interest. The framework is demonstrated through analyzing a 45-story archetype building loca-19 ted in Miami, FL, for which envelope performance is estimated in terms of a suite of probabilistic damage and loss metrics. A comparative study is carried out in order to provide insight into the 21 differences that can occur due to the use of nominal hurricane models. 22
- 23 Keywords: Performance-based Wind Engineering, Hurricanes, Building Envelopes, Probabilistic Damage and Loss Modeling, Extreme
- 24 Winds

1 INTRODUCTION

- 25 Performance-based design (PBD) has been widely accepted as a rational way of assessing risks
- 26 to engineered facilities subjected to natural hazards (Porter, 2003). Over the past decade, signi-
- 27 ficant research effort has been placed on the development of frameworks for the performance-
- 28 based assessment of wind-excited buildings (Ciampoli et al., 2011; Smith and Caracoglia, 2011;

Petrini, F. and Ciampoli, M., 2012; Barbato et al., 2013; Bernardini et al., 2015; Pita et al., 2016; Chuang and Spence, 2017; Cui and Caracoglia, 2018; Ouyang and Spence, 2019; Ierimonti et al., 2019; 30 Micheli et al., 2019; Ouyang and Spence, 2020; Cui and Caracoglia, 2020; Ouyang and Spence, 2021). 31 Most frameworks developed to date assess damage and loss to the building system based on demands 32 estimated exclusively from the structural response (e.g. peak interstory drifts, accelerations) notwithstan-33 ding how a significant portion of envelope damage is generated from local dynamic wind pressure. In 34 an attempt to address this, the authors have recently introduced a PBWE framework in which damage is 35 estimated through a progressive damage analysis in which coupled structural response and wind pressure 36 demands are considered as input to a multi-demand fragility analysis that captures damage state inter-37 dependency (Ouyang and Spence, 2019, 2020, 2021). Similarly to existing PBWE methodologies, this 38 framework adopted a nominal hurricane hazard based on the assumption of a straight (i.e. constant wind 39 direction) and stationary wind event of 1-hour duration. The intensity of the wind event was characterized 40 through the maximum mean hourly wind speed to occur at the building top. Likewise, the intensity of 41 the concurrent rain event was characterized through the maximum horizontal rainfall to occur during the 42 hurricane at the site of interest. While this nominal hurricane setting simplifies subsequent damage and 43 loss analysis, the relative accuracy of performance assessments based on nominal hurricanes, as compared to those carried out considering the full non-straight/-stationary nature of hurricane winds and concurrent 45 rainfall, remains unknown. 46

To fill this knowledge gap, this work develops a PBWE framework for the performance assessment 47 of envelope systems based on describing the full evolution of the hurricane event through parametric 48 49 hurricane models for both the wind and concurrent rainfall fields. In particular, hurricane tracks are described through the probabilistic parametric models outlined in (Vickery and Twisdale, 1995a; Vickery et al., 50 2000b; Cui et al., 2021) while the associated wind fields are described through the 2-dimensional wind 51 field model outlined in (Vickery and Twisdale, 1995b; Vickery et al., 2000a; Jakobsen and Madsen, 2004). 52 These models are subsequently combined with parametric precipitation models (e.g. Lonfat et al., 2007; 53 Snaiki and Wu, 2018; Brackins and Kalyanapu, 2020; Grieser and Jewson, 2012; Geoghegan et al., 2018) 54 that use as input a subset of the hurricane model parameters therefore enabling a probabilistic description 55 of concurrent horizontal rainfall intensity. The consideration of continuously time varying hurricane inputs 56 (i.e. evolving storm track and horizontal rainfall intensity) requires a new set of models for the simulation 57 of the aerodynamic loads and wind-driven rain. To this end, a novel wind-tunnel informed proper orthogo-58 nal decomposition (POD)-based non-straight/-stationary/-Gaussian wind pressure simulation framework 59 is introduced. For the wind-driven rain, the Eulerian-multiphase computational fluid dynamics (CFD) 60 model outlined in (Kubilay et al., 2013, 2015) is adopted with an interpolation scheme within the space of 61 the wind speed and direction therefore allowing for the efficient estimation of the instantaneous rainwater 62 deposition on the building envelope in terms of the continually varying wind speed and direction. 63

To demonstrate the applicability of the framework, a 45-story archetype building located in Miami, FL, is studied in terms of probabilistic performance metrics associated with envelope damages, monetary losses, and water ingress. A comprehensive comparison of the results with those obtained by considering a nominal hurricane setting is also carried out with the aim of better understanding the feasibility of using classic hurricane hazard models in the PBWE of engineered building systems.

2 THE PERFORMANCE-BASED WIND ENGINEERING SETTING

Pioneered by the Pacific Earthquake Engineering Research (PEER) center (Porter, 2003), frameworks for probabilistic performance-based earthquake engineering have been widely adopted as the basis for

developing frameworks for PBWE. The current work is developed based on the recently proposed PBWE framework outlined in (Ouyang and Spence, 2020), the implementation of which enables the estimation of probabilistic building envelope performance metrics of interest to stakeholders (e.g. expected repair costs, expected water ingress, etc.) based on a nominal description of the hurricane hazard. In particular, as detailed in (Ouyang and Spence, 2020), the framework is based characterizing performance through solving the following probabilistic integral:

$$\lambda(dv) = \iiint G(dv|sm)|dG(sm|R_h, \alpha_H, \bar{v}_H)||dG(R_h|\alpha_H, \bar{v}_H)||dG(\alpha_H|\bar{v}_H)||d\lambda(\bar{v}_H)| \tag{1}$$

where G(x|y) is the conditional complementary cumulative distribution function (CCDF) of random variable x given y, sm is the system measure variables (e.g., number of damaged components and amount of water ingress), R_h the mean hourly rainfall intensity, α_H is the wind direction, \bar{v}_H is the maximum mean hourly wind speed measured at a height of interest (e.g., building top), dv is a decision variable threshold of interest (e.g. thresholds related to repair costs, downtime, volume of water ingress), and λ is the mean annual rate of exceeding the threshold of interest, therefore resulting in $\lambda(\bar{v}_H)$ representing the non-directional hurricane hazard curve and $\lambda(dv)$ representing the loss or water ingress curves.

84 For the hurricane framework proposed in this paper, Eq. (1) cannot be directly adopted as the hurricane inputs of wind speed (\bar{v}_H) , wind direction (α_H) , and rainfall intensity (R_h) cannot be treated 85 86 as basic random variables as they are time dependent functions that depend on the evolution of the hurricane. In general, the evolution in time of \bar{v}_H , α_H , and R_h can be related to a vector of basic ran-87 dom variables, Θ , through appropriate parametric models for the hurricane track (Vickery and Twisdale, 88 1995a; Vickery et al., 2000b; Cui et al., 2021), wind field (Vickery and Twisdale, 1995b; Vickery et al., 89 2000a; Jakobsen and Madsen, 2004), and rainfall intensity (Lonfat et al., 2007; Snaiki and Wu, 2018; Brackins and Kalyanapu, 2020; Grieser and Jewson, 2012; Geoghegan et al., 2018). To capture the time 91 92 dependency of \bar{v}_H , α_H , and R_h in the estimation of $\lambda(dv)$, it is therefore necessary to reformulate Eq. (1) explicitly in terms of the vector of basic random variables, Θ , and therefore as:

$$\lambda(dv) = \lambda_e \iint G(dv|sm)|dG(sm|\mathbf{\Theta})||dG(\mathbf{\Theta})|$$
 (2)

where λ_e is the annual recurrence rate of hurricanes of engineering interest while $G(\Theta)$ is the CCDF of Θ . It is important to observe that inherent to estimating the term $G(sm|\Theta)$, is not only the time dependent nature of \bar{v}_H , α_H , and R_h , but also the non-stationary/-straight/-Gaussian wind pressures associated with the time varying wind speed and direction. To retain the explicit dependency on the non-directional hurricane hazard curve and therefore a measure of the overall intensity of a hurricane (used in Sec. 7 to derive an efficient solution strategy for rare events), it is convenient to rewrite Eq. (2) as follows:

$$\lambda(dv) = \iiint G(dv|sm)|dG(sm|\mathbf{\Theta})||dG(\mathbf{\Theta}|\bar{v}_H)||d\lambda(\bar{v}_H)|$$
(3)

where \bar{v}_H is the maximum non-directional mean hourly wind speed to occur at the site of interest over the duration of the hurricane, $G(\Theta|\bar{v}_H)$ is the CCDF of Θ conditional on \bar{v}_H , while $|d\lambda(\bar{v}_H)| = 102 \ \lambda_e f_{\bar{v}_H}(\bar{v}_H) d\bar{v}_H$ with $f_{\bar{v}_H}$ the probability density function (PDF) of \bar{v}_H . The formulation of Eq. (3) decomposes the estimation of envelope performance into three fundamental stages:

- 1. Hurricane hazard analysis, in which the terms $G(\Theta|\bar{v}_H)$ and $\lambda(\bar{v}_H)$ are estimated for different hurricane intensities measured in terms of \bar{v}_H ;
- 106 2. Responses analysis, in which the structural and aerodynamic responses are simulated based on the hurricane parameter vector $\boldsymbol{\Theta}$ to estimate $G(sm|\boldsymbol{\Theta})$;
- 108 3. Loss and consequence analysis, in which the estimates of sm are translated into probabilistic measures of monetary losses and volumes of water ingress through the term G(dv|sm).
- This study is focused on developing a methodology for estimating the performance of envelope systems of engineered buildings through solving Eq. (3). As compared to the frameworks outlined in
- 112 (Ouyang and Spence, 2019, 2020, 2021), which are based on a classic straight/stationary hurricane model
- of nominal 1-hour duration, appropriate hurricane track and wind field models need to be identified (Sec.
- 114 3) for subsequent use as input to new stochastic aerodynamic models that are capable of capturing the
- 115 non-stationary/-straight/-Gaussian wind pressures of full hurricanes (Sec. 4.1). Additionally, the stocha-
- 116 stic simulation scheme outlined in (Ouyang and Spence, 2020, 2021) requires reformulating in terms of
- 117 the parameter vector Θ for enabling rare event simulation in the space of full hurricanes (Sec. 7). Through
- 118 these advances, new knowledge on the envelope performance of engineered buildings during full hurri-
- 119 canes will be created through application to an archetype case study (Sec. 8). To ensure straightforward
- 120 comparison of the results of this study with those reported in (Ouyang and Spence, 2019, 2020, 2021), the
- 121 same case study building will be considered.

3 HURRICANE HAZARD ANALYSIS

122 3.1 Hurricane representations

- Given a site and reference height, H, of interest, the following definitions of hurricane event will be adopted in this work:
- Nominal Hurricane: a site specific stationary (constant time averaged wind speed \bar{v}_H) and straight (constant wind direction α_H) wind event of 1-hour duration with constant concurrent horizontal rainfall intensity R_h . In general, \bar{v}_H is taken as the maximum time-averaged wind speed to occur over the duration of the hurricane at the site of interest, α_H is taken as the direction in which \bar{v}_H occurred, while R_h is taken as the maximum time-averaged rainfall to occur over the duration of the hurricane at the site of interest (Ouyang and Spence, 2019, 2020).
- Full Hurricane: a site specific non-stationary (time varying average wind speed $\bar{v}_H(t)$) and non-straight (time varying wind direction $\alpha_H(t)$) wind event of length equal to the total duration of the hurricane (several hours) with time varying concurrent horizontal rainfall intensity $R_h(t)$.
- 134 From the above definitions, it is clear that the for a given full hurricane, the parameters of the correspon-
- ding nominal hurricane are defined as: $\bar{v}_H = \max[\bar{v}_H(t)]$; α_H extracted from $\alpha_H(t)$ at the time instant at
- which \bar{v}_H occurs; and $R_h = \max[R_h(t)]$. Therefore, given any set of full hurricanes, a corresponding set
- of nominal hurricanes can always be defined. This correspondence will be leveraged in Sec. 8.3.1 when
- 138 comparing the performance of the case study building under full and nominal hurricanes.
- 139 It is important to observe that the straight and stationary nature of the nominal hurricane enable existing
- 140 models to be used for representing the stochastic wind pressures on the building envelope, e.g., those
- outlined in Ouyang and Spence (2020). However, these models cannot be used to represent the stochastic
- 142 wind pressures in full hurricanes due to their non-stationary and non-straight nature. To overcome this,

- 143 Sec. 4.1 will introduce a novel non-straight/-stationary/-Gaussian stochastic wind pressure model. The
- 144 remainder of this section will focus on identifying appropriate parametric models for representing the
- storm track, wind field, and hazard curve of full hurricanes.

146 3.2 Full hurricane model

147 3.2.1 Storm track model

The storm track model outlined in (Vickery and Twisdale, 1995a; Vickery et al., 2000b) is adopted to simulate hurricanes making landfall at a site of interest. In this model, a hurricane risk region is first formed through a circular subregion centered at a location of interest (e.g., building location). Hurricane tracks are subsequently modeled as straight lines crossing the subregion. Within this context, the hurricane lifetime begins when the hurricane center enters the subregion and ends when it leaves the subregion. In this model, the distance vector between the site of interest and the hurricane center, \mathbf{r}_s , at any given time t during the hurricane event is defined as:

$$\mathbf{r}_{s}(t) = \left(\cos\theta \cdot d_{min} - \sin\theta\sqrt{R_{s}^{2} - d_{min}^{2}} + c \cdot \sin\theta \cdot t\right) \cdot \mathbf{e}$$

$$+ \left(-\sin\theta \cdot d_{min} - \cos\theta\sqrt{R_{s}^{2} - d_{min}^{2}} + c \cdot \cos\theta \cdot t\right) \cdot \mathbf{n}$$
(4)

where d_{min} is the minimum distance between the hurricane center and the site of interest (taken positive if the site of interest sits to the left of the hurricane track and negative otherwise), R_s is the diameter of the subregion centered at the site of interest, θ is the angle between the storm track and the north direction, and e and n are the unit vectors pointing towards East and North.

159 3.2.2 Wind field model

160

161

162

163

164

165

167

The parametric model proposed in (Jakobsen and Madsen, 2004) is adopted to model the hurricane wind velocity field. The choice of this model was made as it represents a parametric solution to the wind field model outlined in (Vickery et al., 2000a) that has been carefully validated and used as the basis of the ASCE 7 wind maps. The implementation of this wind field model is coupled with the hurricane track input vector Θ through the initial central pressure difference (Δp_0) and the radius of the maximum wind (r_M). In this model, the mean hourly hurricane wind field at 500 m at time t is solved for the tangential and radial velocity components as:

$$\mathbf{v}_c(r,\beta,t) = v_M(t) \left[\sqrt{r'^{-B} \exp(1 - r'^{-B}) + a^2 r'^2} - ar' \right] (\sin \beta \mathbf{e} - \cos \beta \cdot \mathbf{n})$$
 (5)

$$\mathbf{u}_{c}(r,\beta,t) = \left[\frac{\frac{K}{r} (\frac{\partial v_{c}}{\partial r} + r \frac{\partial^{2} v_{c}}{\partial^{2} r}) - K \frac{v_{c}}{r^{2}} - \frac{C_{d} v_{c}^{2}}{h} \sqrt{1 + \alpha_{M}^{2}}}{\frac{\partial v_{c}}{\partial r} + \frac{v_{c}}{r} + f} \right] (\cos \beta \cdot \mathbf{e} + \sin \beta \cdot \mathbf{n})$$
 (6)

where: \mathbf{v}_c is the tangential component of the velocity field; \mathbf{u}_c is the radial component of the velocity field; B is the Holland number; A is the boundary layer thickness; A is the Coriolis parameter; A are the polar coordinates of a reference system centered at the eye of the hurricane with A = 0 when A points in the positive direction of A; A0.0015) is a drag coefficient related to the boundary layer average

velocity; K is the diffusion coefficient; $r' = r/r_M$; v_M is the maximum tangential velocity given by:

$$v_M(t) = \sqrt{\frac{\lambda B \Delta p(t)}{e \rho_a}} \tag{7}$$

- 173 with ρ_a the air density, e the base of the natural logarithmic function, and λ a coefficient related to the
- 174 advective, diffusive and frictional drag terms in the momentum equations defined as $1/(1+lpha_M^2)$ with
- 175 $\alpha_M = 0.364$; and a is a coefficient given by:

$$a = \frac{fr_M}{2v_M} \tag{8}$$

Based on Eqs. (5) and (6), the wind field vector \mathbf{v}_s at time t can be written as:

$$\mathbf{v}_s(r,\beta,t) = \mathbf{v}_c(r,\beta,t) + \mathbf{u}_c(r,\beta,t) + \exp\left(-\frac{r}{r_G}\right) \cdot \mathbf{c}$$
(9)

- where r_G (~ 500 km) is the environmental length scale defining the extend to which the translation speed
- 178 of the hurricane, c, decays in the radial direction. Based on the above definitions, the mean hourly wind
- 179 speed at a location and height of interest can be estimated through the following transformation:

$$\bar{v}_H(t) = 0.1171 \ln\left(\frac{H}{z_0}\right) \left(\frac{z_0}{z_{01}}\right)^{0.0706} ||\mathbf{v}_s(||\mathbf{r}_s||, \beta_s, t)||$$
 (10)

- 180 where H is the height of interest height (e.g., building height), z_0 is the terrain roughness length at the
- 181 site of interest, z_{01} is the roughness length at 10 m in open terrain, 0.1171 is an adimensional coefficient
- 182 related to transforming wind speeds from 500 m to 10 m in open terrain, and β_s is the angle in polar
- 183 coordinates between the eye of the storm and the the site of interest.
- As the hurricane moves along its track, the wind speed, $\bar{v}_H(t)$, continuously varies due to variations in
- 185 the wind velocity field and relative position of the hurricane center to the site of interest. The correspon-
- 186 ding time varying wind direction, $\alpha_H(t)$, at the site of interest can be determined from $\mathbf{v}_s(||\mathbf{r}_s||, \beta_s, t)$
- 187 estimated for the current wind velocity field.

188 3.2.3 Filling-rate model

- Once hurricanes make landfall, the central pressure difference (Δp) will in general decay resulting in a
- 190 reduction in the wind field and hence the wind speed at the site of interest. To simulate this phenomenon,
- 191 the following filling-rate model is adopted (Vickery and Twisdale, 1995b):

$$\Delta p(t) = \exp\left(-a_f t\right) \Delta p_0 \tag{11}$$

- 192 where an exponential decay is used to model the dissipation of the hurricane central pressure deficit once
- landfall in made. To include uncertainties in the decay rate, the following probabilistic filling constant a_f ,
- 194 dependent on the initial central pressure difference Δp_0 , is considered:

$$a_f = a_0 + a_1 \Delta p_0 + \epsilon_f \tag{12}$$

- where ϵ_f is a zero mean normally distributed error term with standard deviation σ_ϵ while the parameters
- 196 a_1 , a_2 are site specific and model the expected decay. Suggested values for various locations for a_1 , a_2 ,
- 197 and σ_{ϵ} can be found in (Vickery and Twisdale, 1995b). The parameters a_0 , a_1 , and ϵ_f are included in the
- 198 hurricane input parameter vector Θ .

199 3.2.4 Precipitation model

- 200 To model the concurrent rainfall, the IPET (Interagency Performance Evaluation Task) parametric pre-
- 201 cipitation model, developed based on the National Aeronautics and Space Administration's Tropical
- 202 Rainfall Measuring Mission database, is adopted (Lonfat et al., 2004; Chen et al., 2006). Comparative
- 203 studies have suggested this models is superior to other commonly used parametric rainfall models
- 204 (Lonfat et al., 2004; Brackins and Kalyanapu, 2020). From the IPET model, the evolution of the mean
- 205 hourly horizontal rainfall, $R_h(t)$, can be estimated at the site of interest directly from the hurricane
- 206 parameters $\Delta p(t)$, $r_s(t)$ and r_M at any given time, t, through the following expression:

$$R_h(t) = \begin{cases} 1.14 + 0.12\Delta p(t); & r_s(t) \le r_M \\ (1.14 + 0.12\Delta p(t)) \exp\left(-0.3\left(\frac{r_s(t) - r_M}{r_M}\right)\right); & r_s(t) > r_M \end{cases}$$
(13)

- 207 where Δp is in millibars, R_h is in h/mm, and $r_s(t)$ and r_M are in kilometers. The value calculated by
- 208 Eq. (13) provides the symmetric component of the rainfall field. To estimate the asymmetric component,
- 209 $R_h(t)$ can be multiplied by a factor of 1.5 if the site of interest is in the northern hemisphere and to the
- 210 right of the hurricane track (0.5 if it is to the left).

211 3.3 Hazard curve of the full hurricane model

- The intensity of each hurricane is measured through the maximum mean hourly wind speed, \bar{v}_H , to
- 213 occur at the site of interest at height H during the passage of a hurricane. The choice of \bar{v}_H as an intensity
- 214 measure is convenient as it allows direct comparison between performance assessments carried out using
- 215 a nominal or full hurricane representation. As will be outlined in Sec. 7, it also allows for the definition of
- 216 a conditional stochastic simulation strategy that enables the efficient estimation of failure rates associated
- 217 with rare events.
- Following this definition, the performance assessment of envelope systems through Eq. (3) relies on an
- 219 accurate estimation of the hazard curve $\lambda(\bar{v}_H)$. In particular, unlike the nominal case where \bar{v}_H is treated
- 220 as an independent random variable to be characterized alongside wind direction, \bar{v}_H is dependent on the
- 221 hurricane track input parameters Θ . In other words, the probability density function (PDF) of \bar{v}_H takes
- 222 the form:

$$f_{\hat{v}_H}(\bar{v}_H) = \int_{\mathbf{\Theta}} f_{\bar{v}_H|\mathbf{\Theta}}(\bar{v}_H|\mathbf{\Theta}) f_{\mathbf{\Theta}}(\mathbf{\Theta}) d\mathbf{\Theta}$$
(14)

- 223 where the components of Θ are the initial central pressure difference Δp_0 , translation speed c, size of the
- 224 hurricane r_M , approach angle θ , shortest distance d_{min} between site of interest and hurricane track, and
- 225 the coefficients a_0 , a_1 and ϵ_f of the filling-rate model, $f_{\hat{v}_H}$ is the PDF of \hat{v}_H , $f_{\bar{v}_H|\Theta}$ is the PDF of \hat{v}_H
- 226 conditional on Θ , and f_{Θ} is the joint PDF of the components of Θ . From $f_{\hat{v}_H}(\bar{v}_H)$, the hazard curve is
- 227 defined as:

$$\lambda(\bar{v}_H) = \lambda_e \int_{\bar{v}_H}^{+\infty} f_{\hat{v}_H}(v) dv \tag{15}$$

where λ_e is the mean annual recurrence rate of hurricanes of engineering interest.

4 RESPONSE ANALYSIS: ENVELOPE ACTIONS

229 4.1 Non-stationary/-straight/-Gaussian external pressure

230 4.1.1 Overview

Base on the straight and stationary wind pressure simulation model outlined in (Ouyang and Spence, 231 2020), a non-stationary/-straight wind pressure model is developed to capture the effects on the aerody-232 namic pressures of the continuously varying wind speed and direction associated with full hurricanes. 233 The main steps of the model are outlined in the conceptual flowchart of Figure 1. The model is cali-234 brated to data in the form of vectors of model-scale surface pressure coefficients $C_{p,e,M}(t_M)$, with t_M 235 is the model-scale time, collected in wind tunnel tests where stationary/straight but non-Gaussian pres-236 sures are measured at a grid of sensors on the model surface for a discrete set of wind directions (e.g., 237 $\{10^{\circ}, 20^{\circ}, ..., 360^{\circ}\}$). To reconcile the discrete wind directions of the wind tunnel data with the continu-238 ously varying wind directions of the hurricane track, these last are transformed into a piece-wise discrete 239 representation, as illustrated in step (I) of **Figure 1**, where a set of segments with constant wind directi-240 ons are defined. In step (II), model-scale stationary/straight but non-Gaussian wind pressure coefficient 241 vector processes, $\mathbf{C}_{p,e,M}^{(i)}(t_M)$, are generated for each segment through the straight/stationary but non-Gaussian models outlined in (Ouyang and Spence, 2020). In step (III) the continuous wind directions are 242 243 244 approximated through a piece-wise linear representation to which the segments of straight/stationary and 245 non-Gaussian pressures are merged therefore leading to a non-stationary/-straight/-Gaussian representation of the pressure coefficient vector process, $C_{p,e,M}(t_M)$, for the full hurricane event at model-scale. 246 Finally, $C_{p,e,M}(t_M)$ is mapped back to the building-scale time in step (IV) and translated to the 247 248 non-stationary/-straight/-Gaussian process, $\mathbf{p}_e(t)$, in step (V).

249 4.1.2 Procedure

In the following, further details of each step of the model outlined in **Figure 1** are provided.

251 **Step I**

The continuous wind direction history, $\alpha_H(t)$, is first discretized into a set of segments with each segment representing a straight wind event. This discretization can be expressed as:

$$\bar{\alpha}_H(t) = \min\left(\frac{\alpha_H(t)}{\Delta \alpha}\right) \Delta \alpha$$
 (16)

where $\bar{\alpha}_H(t)$ is the discretized wind direction history, nint is the function which returns a number rounded to the nearest integer, $\Delta\alpha$ is the direction step size of the wind tunnel tunnel data (e.g., $\Delta\alpha=10^\circ$). Each segment, $\bar{\alpha}_H^{(i)}(t)$, represents a straight wind event, where $i\in\{1,2,...,N_{seg}\}$ with N_{seg} the total number of segments defining $\bar{\alpha}_H(t)$. Within the segment $\bar{\alpha}_H^{(i)}(t)$, the mid-time is denoted by $T_m^{(i)}$ (e.g., the red dots in **Figure 1**) with the start and end time denoted by $T_s^{(i)}$ and $T_e^{(i)}$. To form the transition region, each segment is further extended on both ends up to the mid-times of the nearby segments (i.e. the ith segment is extended to $T_m^{(i-1)}$ and $T_m^{(i+1)}$ with the boundary cases of i=1 and $i=N_{seg}$ treated by only extending one end).

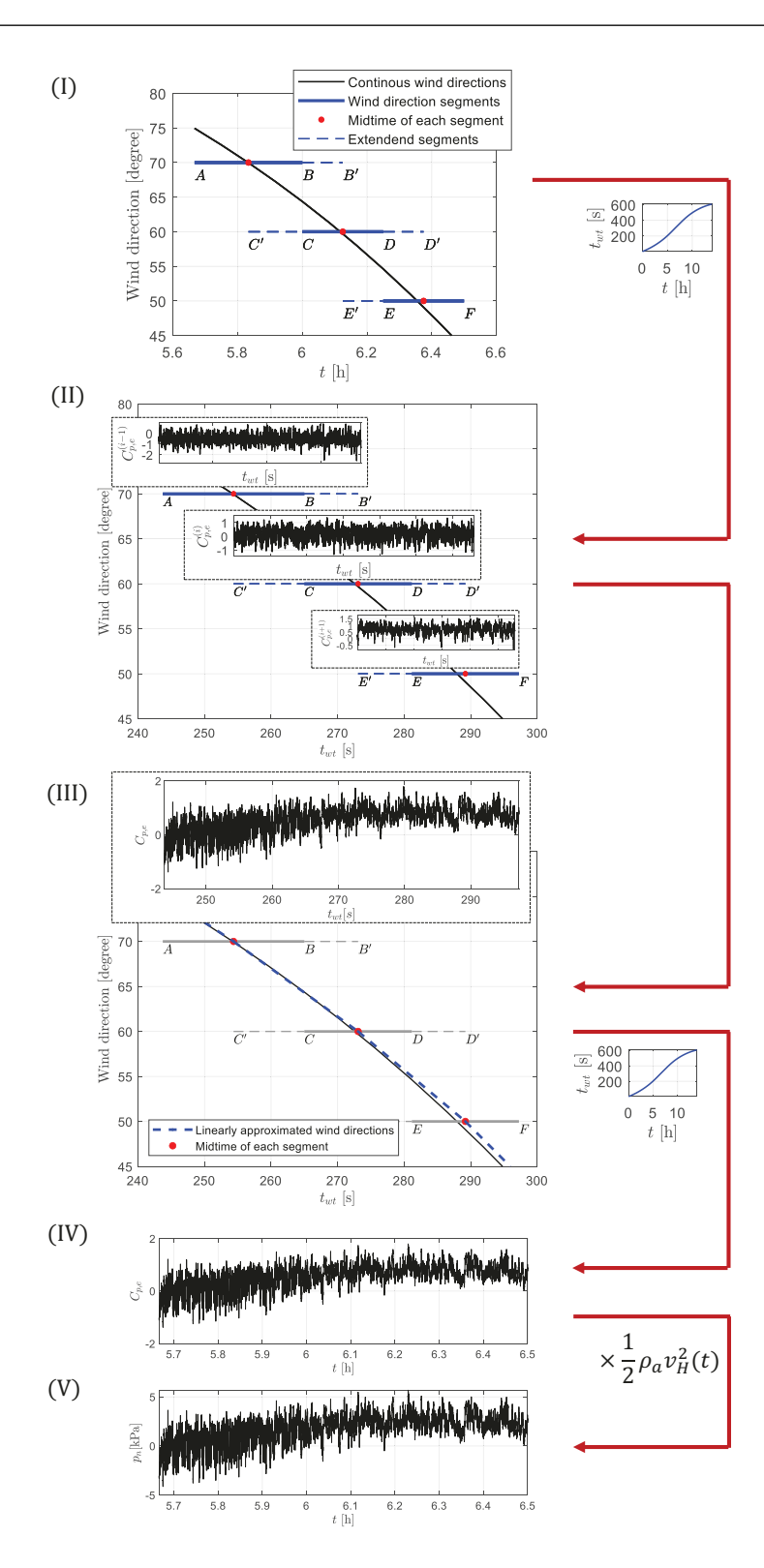


Figure 1. Conceptual flowchart of the non-stationary/-straight/-Gaussian stochastic wind pressure simulation model.

262 **Step II**

In this step, a wind pressure coefficient vector process, $\mathbf{C}_{p,e,M}^{(i)}(t_M)$, is generated for each extended segment at the model-scale. To obtain the total duration of each extended segment at model-scale, the

following nonlinear time-scale mapping from t to t_M is derived base on Strouhal number matching:

$$t_M(t) = \frac{\gamma_H}{\bar{v}_M} \int_0^t \bar{v}_H(u) du \tag{17}$$

with γ_H is the ratio of model to full scale height, \bar{v}_M is the mean wind speed used during the wind tunnel tests. Based on Eq. (17), the duration of the ith extended segment can be calculated from: 267

$$T_{seg}^{(i)} = \begin{cases} t_M(T_m^{(i+1)}) - t_M(T_s^{(i)}) \text{ if } i = 1\\ t_M(T_e^{(i)}) - t_M(T_m^{(i-1)}) \text{ if } i = N_{seg}\\ t_M(T_m^{(i+1)}) - t_M(T_m^{(i-1)}) \text{ otherwise} \end{cases}$$
(18)

with $T_{seq}^{(i)}$ the duration of the *i*th extended segment.

- Through Eq. (18), the duration of each extended segment is calculated and used to simulate the sta-269
- tionary/straight but non-Gaussian wind pressure coefficient vector processes, $\mathbf{C}_{p,e,M}^{(i)}(t_M)$, through the models outlined in (Ouyang and Spence, 2020). The maximum possible sampling frequency (dictated by 270
- 271
- the wind tunnel data) should be chosen in generating $\mathbf{C}_{p,e,M}^{(i)}(t_M)$ to minimize any interpolation errors in
- 273 Step (V).

Step III 274

- From the stationary wind pressure coefficient vector processes $\mathbf{C}_{p,e,M}^{(i)}(t_M)$ of step (II), a filter-based transition model is introduced to merge the segments into a non-stationary/-straight/-Gaussian wind 275
- 276
- pressure coefficient vector process $C_{p,e,M}(t_M)$. To implement the transition, the stationary processes
- $\mathbf{C}_{p,e,M}^{(i)}(t_M)$ are decomposed into a time-averaged component, $\overline{\mathbf{C}}_{p,e,M}^{(i)}(t_M)$, and a fluctuation component, $\widetilde{\mathbf{C}}_{p,e,M}^{(i)}(t_M)$, such that:

$$\mathbf{C}_{p,e,M}^{(i)}(t_M) = \overline{\mathbf{C}}_{p,e,M}^{(i)}(t_M) + \widetilde{\mathbf{C}}_{p,e,M}^{(i)}(t_M)$$

$$\tag{19}$$

The following linear ramping-based filter is then applied to each time-averaged component:

$$\psi^{(i)}(t_M) = \begin{cases} \frac{t_M - T_{M,m}^{(i)}}{T_{M,m}^{(i+1)} - T_{M,m}^{(i)}} & \text{if } t_M > T_{M,m}^{(i)} \\ \frac{T_{M,m}^{(i)} - t_M}{T_{M,m}^{(i)} - T_{M,m}^{(i-1)}} & \text{if } t_M \le T_{M,m}^{(i)} \end{cases}$$

$$(20)$$

where $T_{M,m}^{(i)}$ is the mid-time of the ith segment in model-scale time. Based on this linear filter, the merged time-averaged components, with $t_M \in [T_{M,m}^{(i)}, T_{M,m}^{(i+1)}]$, are defined as:

$$\overline{\mathbf{C}}_{p,e,M}(t_M) = \psi^{(i)}(t_M)\overline{\mathbf{C}}_{p,e,M}^{(i)}(t_M) + \psi^{(i+1)}(t_M)\overline{\mathbf{C}}_{p,e,M}^{(i+1)}(t_M)$$
(21)

To merge the fluctuation components, $\widetilde{\mathbf{C}}_{p,e,M}^{(i)}(t_M)$, a nonlinear ramping-based filter in the form of the square root of $\psi^{(i)}$ is applied, with $t_M \in [T_{M,m}^{(i)}, T_{M,m}^{(i+1)}]$, as follows: 283 284

$$\widetilde{\mathbf{C}}_{p,e,M}(t_M) = \sqrt{\psi^{(i)}(t_M)} \widetilde{\mathbf{C}}_{p,e,M}^{(i)}(t_M) + \sqrt{\psi^{(i+1)}(t_M)} \widetilde{\mathbf{C}}_{p,e,M}^{(i+1)}(t_M)$$
(22)

By iterating over all segments, with special boundary consideration for i=1 and $i=N_{seq}$, $\overline{\mathbf{C}}_{p,e,M}(t_M)$

and $\widetilde{\mathbf{C}}_{p,e,M}(t_M)$ are estimated for the entire hurricane track. The final non-stationary/-straight/-Gaussian wind pressure coefficient vector process is then obtained as:

$$\mathbf{C}_{p,e,M}(t_M) = \overline{\mathbf{C}}_{p,e,M}(t_M) + \widetilde{\mathbf{C}}_{p,e,M}(t_M)$$
(23)

Through the transition model outlined above, the merged wind pressure vector process will have second order statistics (auto- and cross-correlation functions) that vary following a near linear relationship betw- een the wind directions in which wind tunnel data is available. Inherent to this transition model is the capture of non-Gaussianity in $\mathbf{C}_{p,e,M}(t_M)$ that matches those observed in the wind tunnel for the discrete wind directions at which wind tunnel tests were performed.

293 **Step IV**

294 To generate the wind pressure vector process at building-scale with a target constant sampling frequency, 295 the model-scale wind pressure coefficient vector process needs to be sampled with a non-uniform sam-296 pling frequency due to the continuously varying wind speed $v_H(t)$. This non-uniform sampling is achieved 297 through a model-scale interpolation scheme, where the uniform time samples t_l , with $l \in \{1, 2, ..., N_l\}$ and N_l the total number of uniform samples at building-scale, are mapped to the model-scale through Eq. 298 (17). This leads to a non-uniform space of model scale time samples $t_M(t_l)$ that are evaluated through 299 300 interpolation. The discrete representation of the building-scale non-stationary/-straight/-Gaussian pressure coefficient vector process, $C_{p,e}(t_l)$, is defined as: 301

$$\mathbf{C}_{p,e}(t_l) = \mathbf{C}_{p,e,M}(t_M(t_l)) \tag{24}$$

302 Step V

From the pressure coefficient processes of Eq. (24), the non-stationary/-straight/-Gaussian external pressures can be estimated as:

$$\mathbf{p}_e(t_l) = \frac{1}{2} \rho_a v_H^2(t_l) \mathbf{C}_{p,e}(t_l)$$
(25)

where \mathbf{p}_e is the vector of the non-stationary/-straight/-Gaussian pressure processes at the sensor grid locations at full scale. To estimate the pressure processes at a location, identified by the coordinate ξ_{xyz} , on the building envelope where direct measurements where not carried out, 2D interpolation with extrapolation can be used (Ouyang and Spence, 2019, 2020).

309 4.2 Wind-driven rain

310 The simulation of the time-dependent wind-driven rain is developed through the extension of the nominal wind-driven rain model outlined in (Ouyang and Spence, 2020). For the nominal hurricane, constant 311 wind-driven rain is simulated through the 3D steady Reyolds-averaged Navier-Stokes (RANS) equations-312 based Eulerian multiphase (EM) model proposed in (Huang and Li, 2012; Kubilay et al., 2013, 2017). 313 314 The implementation of this framework consists of two steps: (1) the RANS equations with a realizable $k-\epsilon$ turbulence model are solved for the steady-state wind field around the building; and (2) based on the 315 steady-state solution from the first step, the EM model is implemented with the $k-\epsilon$ turbulence model 316 to solve for wind-dispersed rain phases. In particular, each rain phase represents a phase flow problem for 317 a group of raindrops with diameters in a predefined range. The solution of the EM model gives a vector 318

of normalized specific catch ratios, $\bar{\eta}(\xi_{xyz})$, for all rain phases at each location, ξ_{xyz} , of interest. The corresponding wind-driven rain can then be directly calculated based on the rainfall intensity, R_h , and the associated conditional raindrop diameter distribution.

To model the time-dependency of the wind-driven rain due to the continuously varying wind speed and 322 direction the specific catch ratios would need to be continuously solved in time. This poses a signifi-323 cant computational issue as this would in general imply the need to solve RANS-based EM models for 324 a sequence of wind speeds and directions for each storm track of interest. To overcome this issue, an 325 interpolation-based approach is adopted, where the specific catch ratios at each envelope point of inte-326 rest, $\bar{\eta}(\xi_{xyz})$, are pre-computed for a predetermined grid of wind directions, α_H , and wind speeds, v_H . 327 The time-dependency of $\bar{\eta}(\xi_{xyz})$ can then be efficiently estimated through instantaneous interpolation at 328 $\alpha_H(t)$ and $v_H(t)$. Based on this approach, the time-dependent wind-driven rain intensity at each envelope 329 location of interest, $R_{wdr}(\xi_{xyz}, t)$, is estimated as: 330

$$R_{wdr}(\xi_{xyz}, t) = \Phi^{T}(t)\bar{\boldsymbol{\eta}}(\xi_{xyz}, \alpha_{H}(t), v_{H}(t))$$
(26)

where $\Phi(t)$ is a weighting vector whose kth component is defined as:

$$\Phi_k(t) = R_h(t)\Delta d_k f_h\left(d_k|R_h(t)\right) \tag{27}$$

with Δd_k is the raindrop diameter range of the kth rain phase, d_k is the median raindrop diameter in the kth rain phase, and kth rain phase phase

5 RESPONSE ANALYSIS: SYSTEM ANALYSIS

Based on the envelope actions, demands in terms of dynamic story drifts and local net dynamic pressures can be estimated through the adoption of the models outlined in (Ouyang and Spence, 2020). Based on these demands, system measures, sm, associated with the final damage states of each vulnerable envelope component and subsequent water ingress can be evaluated. As will be briefly outlined below, the use of the models outlined in (Ouyang and Spence, 2020), enables not only the capture of the interdependencies between demands and damages, but also the progressive nature of wind induced damage.

340 **5.1 Demands**

341 5.1.1 Structural response

Based on the results reported in (Ouyang and Spence, 2021), the structural system is assumed to respond elastically. The dynamic response of the structural system can therefore be estimated through solving the following modal equations:

$$\ddot{q}_i(t) + 2\omega_i \zeta_i \dot{q}_i(t) + \omega_i^2 q_i(t) = Q_i^{\mathcal{N}}(t)$$
(28)

where q_i , \dot{q}_i and \ddot{q}_i are the displacement, velocity and acceleration associated with the *i*th dynamic mode; 346 ω_i and ζ_i are the circular frequency and modal damping ratio of the *i*th mode, while $Q_i^{\mathcal{N}}(t)$ is the non-347 stationary/-straight/-Gaussian generalized force of the *i*th mode estimated as:

$$Q_i^{\mathcal{N}}(t) = \frac{\phi_i^T}{\phi_i^T \mathbf{M} \phi_i} \tilde{\mathbf{f}}_{\mathcal{N}}(t)$$
 (29)

348 where ϕ_i is the *i*th mode shape; M is the structural mass matrix; and $\tilde{\mathbf{f}}_{\mathcal{N}}(t)$ is the dynamic forcing vector 349 evaluated through integrating the non-stationary/-straight/-Gaussian pressures of Eq. (25).

From the solution of Eq. (28), the dynamic structural response can be approximated from the first N_m modes as:

$$\mathbf{x}(t) \approx \sum_{i=1}^{N_m} \phi_i q_i(t) \tag{30}$$

352 Dynamic story drift, Dr(t), at any location of interest can then be directly estimated through linear 353 combination of the appropriate components of $\mathbf{x}(t)$.

354 5.1.2 Net dynamic pressure

The net pressure demands at an envelope location ξ_{xyz} of interest, $p_n(t, \xi_{xyz})$, are evaluated as:

$$p_n(t, \xi_{xyz}) = p_e(t, \xi_{xyz}) - p_i(t, \xi_{xyz})$$
 (31)

where $p_e(t, \xi_{xyz})$ is the external pressure estimated through the models of Sec. 4.1 at ξ_{xyz} while $p_i(t, \xi_{xyz})$ 356 are the corresponding internal pressures. To estimate the dynamic internal pressures $p_i(t, \xi_{xyz})$, the interior 357 of the building is modeled as a system of interconnected compartments. Initially, the building is considered 358 359 enclosed with negligible internal pressurization. During the hurricane, openings can be created in the envelope due to component damages, which allows air to flow into or out of the building triggering 360 dynamic internal pressures in all compartments that are connected through an internal opening. To solve 361 the transient air flows, the internal pressure model outlined in (Ouyang and Spence, 2019) is adopted, in 362 which the air velocity at each opening is described through the unsteady-isentropic form of the Bernoulli 363 equation (Vickery and Bloxham, 1992; Guha et al., 2011; Yu et al., 2008). To treat the time dependency 364 of \bar{v}_H , the dynamic internal pressures, $p_i(t, \xi_{xyz})$, at each opening (external/internal or internal/internal) 365 are directly estimated through solving of system nonlinear equations (one for each opening) derived based 366 on the principle of mass conservation. A 4th-order Runge-Kutta scheme can be used to solve the system 367 where, at each time step, the pressure-induced damages are iteratively updated until dynamic equilibrium 368 is achieved. 369

It is important to observe that in solving for $p_i(t, \xi_{xyz})$ the current drift induced damage state of each envelope component must be considered. This couples not only the structural and pressure demands (e.g., a drift induced damage to the envelope can cause air flow therefore effecting the internal pressure), but also the demand and damage analysis (e.g., the occurrence of a drift or pressure induced damage state can effect internal pressures). It should also be observed that damage to the envelope is progressive in nature as it accumulates over the duration of the event.

376 **5.2 System measures**

377 5.2.1 Component damages

To model the damage susceptibility of the ith envelope component to N_{Dr}^i drift induced and N_P^i pressure-induced damage states, suites of N_{Dr}^i and N_P^i sequential damage thresholds are defined: 380 $\mathbf{C}_P^i = \{C_{P_1}^i \leq C_{P_2}^i \ldots \leq C_{P_{N_P}}^i\}$ and $\mathbf{C}_{Dr}^i = \{C_{Dr_1}^i \leq C_{Dr_2}^i \ldots \leq C_{Dr_{N_{Dr}}}^i\}$. The randomness in the thresholds are modeled through corresponding suites of sequential fragility functions. At a given time step, 382 \hat{t} , all component thresholds are compared with the current story drift demand, $Dr^i(\hat{t})$, and net pressure demand $p_n(\hat{t}, \xi_{xuz}^i)$, where the largest exceeded threshold defines the current pressure and/or drift induced

damage state. To model potential coupling between drift and pressure induced damage states (e.g., the 384 occurrence of a drift induced damage state could effect the capacity of the component to resist net pres-385 sure and viceversa), the thresholds of a suite of coupled damage states are probabilistically degenerated 386 upon the occurrence of the coupled damage state. The final damage states of each envelope component 387 represent the system measures of interest. 388

5.2.2 Water ingress

389

390 391

392

393 394

395 396

397

398

399

400

401

402

403

404

405

406

407

408

409

410

411

412

413

414

415

The concurrent rainfall leads to the deposition of rainwater on the envelope. Damage to the envelope can then lead to water ingress. To estimate the volume of water ingress, the flow rate at each opening can be estimated directly from $R_{wdr}(\xi_{xuz},t)$, estimated through the models of Sec. 4.2, and the steadystate water runoff solution derived in (Ouyang and Spence, 2019). From the flow rate at each opening, the total volume of water entering through an opening at a given time, \hat{t} , can be estimated by integrating the flow rate from the time the opening first occurred, i.e. the time at which the damage causing the opening occurred. Through the implementation of the water ingress model, the time traces of total volume of water entering through each opening can be estimated.

LOSS AND CONSEQUENCE ANALYSIS 6

To translate the final damage states of each envelope component into repair costs and actions, the concept of unit loss function (ULF), as defined in (Federal Emergency Management Agency (FEMA), 2012b), is adopted. Specifically, the ULF defines the repair cost as a monotonically decreasing function with respect to the total number of components in a given damage state. To consider economies of scale, a minimum quantity, Q_{min} , is defined as the lower limit below which economies of scale do not take effect. Likewise, a maximum quantity, Q_{max} , is defined as the upper limit after which economies scale no longer occur. To include uncertainty in the loss estimation, the value given by the ULF is taken as the expected value of a lognormal random variable with assigned dispersion. This dispersion accounts, to a certain extent, for the many complexities involved in estimating repair cost and time following a hurricane, e.g., administrative backlogs, demand surge, lack of materials, and shortage of labor. Through ULFs, each envelope damage state can be converted to estimates of the repair cost (or time). The evaluation of the total system level repair cost, i.e. the decision variable (dv), can then be evaluated through summing all envelope component repair costs. This scheme can also be used to estimate downtimes associated with repair actions. Similarly, the system-level consequence of envelope damage related to total volume of water ingress can be assessed by summing the volumes of water ingress at each damaged envelope component. Additionally, the information provided by the framework on water ingress would support the use of models for estimating damage to the interior components and contents through providing detailed information on the water paths and flow rates at each damaged envelope component.

7 SIMULATION STRATEGY

- The evaluation of the envelope system performance relies on the possibility of efficiently solving Eq. (3). Because the failure rates of interest to this work are small, i.e. related to rare events, and the models 417 used to characterize performance are computational intense, direct Monte Carlo (MC) methods are gene-418 rally intractable. To overcome this, a conditional stochastic simulation scheme, that integrates subset 419
- simulation (Au and Beck, 2001), is developed. The approach is based on using \bar{v}_H as an indicator of hur-420
- ricane intensity. The hazard curve is then divided into $N_{\bar{v}_H}$ mutually exclusive and collectively exhaustive 421
- hazard intervals with each interval representing a set of sub-events of intensity measured over intervals 422

429

442

443

444

445

446

447

448

449

450

451

452

453

454

455

456

457 458

459

of maximum mean hourly wind speed. The performance within each sub-event is evaluated using direct MC methods. The samples for each sub-event are generated through a hybrid simulation technique in which hurricane track samples, i.e. realizations of Θ conditional on the sub-event, are efficiently generated through Markov chain Monte Carlo (MCMC) algorithms and combined with randomly sampled sets of model parameters (e.g., the component thresholds and modal damping ratios). Following this strategy, Eq. (3) is reformulated through the total probability theorem as:

$$\lambda(dv) = \lambda_e \sum_{k=1}^{N_{\bar{v}_H}} \left[\iint G(dv|sm) |dG(sm|\mathbf{\Theta})| |dG(\mathbf{\Theta}|E_{\bar{v}_H,k})| \right] P(E_{\bar{v}_H,k})$$
(32)

bound wind speed defining the kth interval, where $\bar{v}_{H,k}^U=+\infty$ for $k=N_{\bar{v}_H};\,P(E_{\bar{v}_H,k})$ is the probability 430 of a hurricane sample belonging to $E_{\bar{v}_H,k}$ (which can be directly estimated from the hazard curve); $N_{\bar{v}_H}$ is 431 the total number of sub-events; and λ_e is the annual recurrence rate of hurricanes of engineering interest. 432 To evaluate Eq. (32) through the approach outlined above, subset simulation is first used to estimate 433 the hazard curve, $\lambda(\bar{v}_H)$, through sampling the space of Θ while using \bar{v}_H as the response of interest. In 434 particular, it is convenient to select the lower and upper bound wind speeds for each sub-event based on 435 the thresholds of \bar{v}_H identified during the implementation of subset simulation. In this way, the number 436 of intervals will depend on the target exceedance probability set for the lower bound of the last interval 437 and the intermediate probability, P_s , used in calibrating the subset simulation algorithm. Furthermore, 438 the probabilities $P(E_{\bar{v}_H,k})$ can be directly estimated from P_s . The number of samples used for each 439 440 conditional failure event of the subset simulation will dictate the maximum number of samples that can be used to evaluated the term in square brackets of Eq. (32) through MC simulation. Therefore, the number 441

with $E_{\bar{v}_H,k}$ is the kth sub-event defined as $\bar{v}_H \in [\bar{v}_{H,k}^L, \bar{v}_{H,k}^U)$ with $\bar{v}_{H,k}^L$ and $\bar{v}_{H,k}^U$ the lower- and upper-

8 CASE STUDY

8.1 Building system

of samples should be chosen to provide adequate resolution.

To illustrate the proposed framework while also studying the differences between performance assessments carried out using nominal as opposed to full hurricane hazard models, the archetype building outlined (Ouyang and Spence, 2020) with location Miami, FL, is considered. As shown in **Figure 2**, the building is a rectangular 45-story steel structure with central core and symmetric X-bracing. The total height of the structure is 180 m with a constant floor height of 4 m. The structural system was designed to satisfy typical serviceability and life safety requirements. The first 10 vibration modes were considered adequate for representing the dynamic response. The first three natural frequencies were 1.30 rad/s, 1.67 rad/s, and 2.70 rad/s respectively. The damageable components considered in the case study are the dualpane laminated glazing units of size of 1.2×2 m². The thickness of each laminated pane is taken as 6 mm. Each floor has 180 units with 60 units on the south (north) face and 30 units on the east (west) face, which results in a total of 8100 units for the entire building. To calibrate the damage model of Sec. 5.2.1, two drift-induced damages states (defined as hairline cracking, DS_{Dr_1} , and the glass cracking, DS_{Dr_2}) and one pressure-induced damage state $DS_{P_{60}}$ (defined as full loss of the window panes) are defined with random thresholds calibrated through the fragility functions reported in Table 1. The dual panes are considered fully correlated in terms of capacity and to work in parallel when resisting net pressure, modeled as equivalent over a duration of 60 s (Ouyang and Spence, 2020). Further details on the case study building,

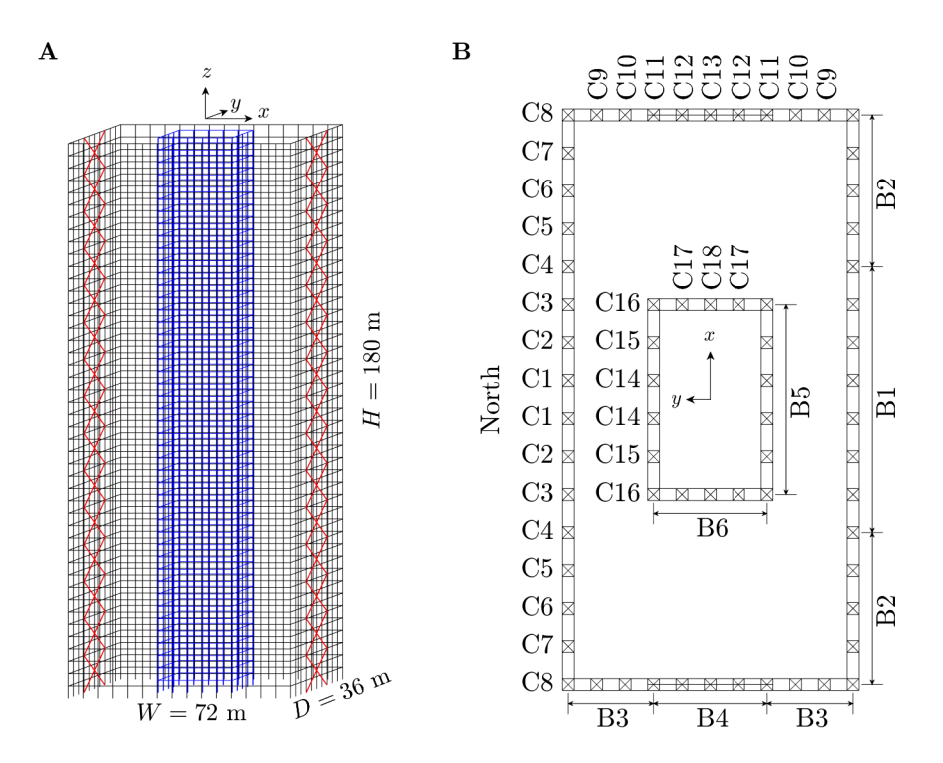


Figure 2. (A) Three-dimensional illustration of the 45-story structure; (B) plan view indicating the floor member layout (B = beam and C = column) and North.

including the pre-computed wind-driven rain simulations for calibrating Eq. (26), can be found in the Appendix.

Table 1. Fragility functions for each glazing unit.

State		Dispersion	Mean	Std	Unit
$\overline{DS_{Dr_1}}$	0.021	0.45	-	-	rad
DS_{Dr_2}	0.024	0.45	-	-	rad
$DS_{P_{60}}^{2}*$	-	-	5.29	0.91	kPa

^{*}demand in terms of 60 s equivalent net pressure.

462 8.2 Hurricane hazard

463

464

465

466

467

468

469

470 471

472

473

To calibrate the parametric hurricane model of Sec. 3.2.1, and therefore the vector Θ , to Miami, a subregion diameter of $R_s=500$ km was considered while the probabilistic characteristics of the components of Θ followed those suggested in (Vickery and Twisdale, 1995a). In converting mean hourly wind speeds at 500 m to H=180 m (i.e. building top) through Eq. (10), values of $z_0=1.28$ m and $z_{01}=0.03$ m were considered. The aerodynamic model of Sec. 4.1.2 was calibrated to a data set of the Tokyo Polytechnic University (TPU) wind tunnel pressure database (Tokyo Polytechnic University, 2008). This data is used to calibrate the stationary/straight but non-Gaussian wind pressure coefficient processes, $C_{p,e,M}(t_M)$, at model-scale. For the data set considered, the ratio of tunnel model height to building height, γ_H , was 1/360 while the mean wind speed at model height during the wind tunnel tests was $\bar{v}_M=11.11$ m/s. The turbulence intensity was 25% while the wind speed profile had a power law coefficient of 1/4. During the tests, transient pressure coefficients were simultaneously measured at 510 pressure taps located over the

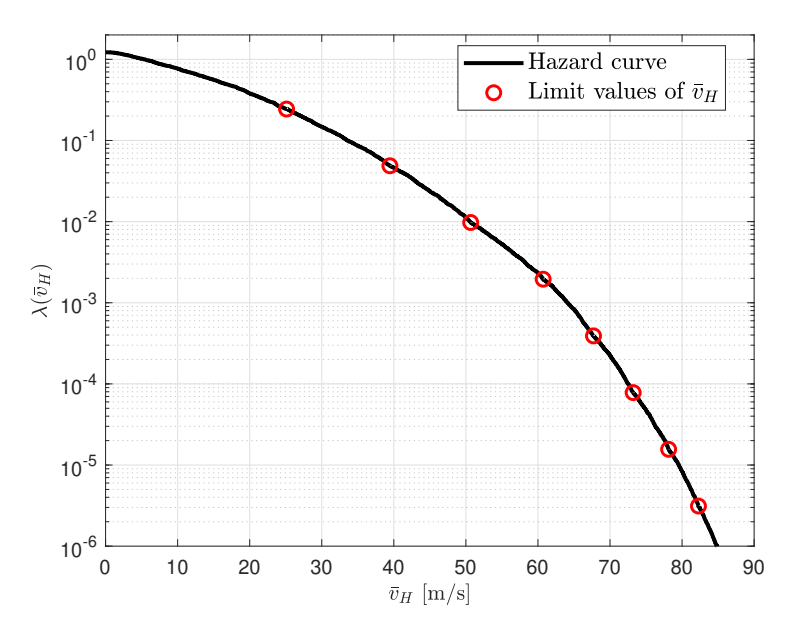


Figure 3. The estimated hurricane hazard curve.

- building surface with a constant sampling frequency of 1000 Hz and a wind direction increment of 10°.
- Based on $C_{p,e,M}(t_M)$, realizations of the non-stationary/-straight/-Gaussian wind pressure vector process,
- 476 $C_{p,e}(t)$, were generated through the five-step procedure of Sec. 4.1.2.

477 As defined in Sec. 3.2.1, each sample of Θ uniquely determines the hurricane track of a full hurricane. To estimate the hazard curve through subset simulation, an intermediate probability of $P_s = 0.2$ 478 was chosen together with $N_{\overline{v}_H}=9$ conditional failure events. Considering how $\lambda_e=1.22$ for Miami 479 (Vickery and Twisdale, 1995a), this leads to a lower bound wind speed with an annual exceedance rate 480 of $\lambda_e(P_s)^8 = 3.123 \times 10^{-6}$, i.e. a mean recurrence interval of over 300,000 years, which is considered 481 adequate for evaluating the performance of the system for PBWE design scenarios. Within each subset, 482 $N_s = 1300$ samples of Θ are considered. In running the MCMC Metropolis Hasting algorithm, a univari-483 ate normal distribution with zero mean and standard deviation of 0.5 was considered as the proposal pdf. 484 The choice of $N_s = 1300$ leads to $N_s(1 - P_s) = 1040$ hurricane samples for the subsequent MC analysis 485 necessary for evaluating Eq. (32) through the procedure of Sec. 7. The final hazard curve is reported in 486 487 Figure 3.

488 **8.3 Results**

496

497

498

489 8.3.1 Preamble

To enable the comparison between the full hurricane model of this work and a classic nominal hurricane setting, for each full hurricane sample, a nominal hurricane is also generated based on the maximum wind speed \bar{v}_H , with associated direction α_H , and the maximum rainfall intensity to occur over the duration of the full hurricane. For both nominal and full hurricanes, a uniform time step of $\Delta t = 0.5$ s at building-scale is used.

495 8.3.2 Discussion on a single event

To illustrate and discuss the evolution of damage during a full hurricane event, a single hurricane event is analyzed in detail in this section. The event corresponds to a category five hurricane on the Saffir-Simpson scale (Taylor et al., 2010), with a maximum mean hourly wind speed at the building top of 67.7 m/s. The

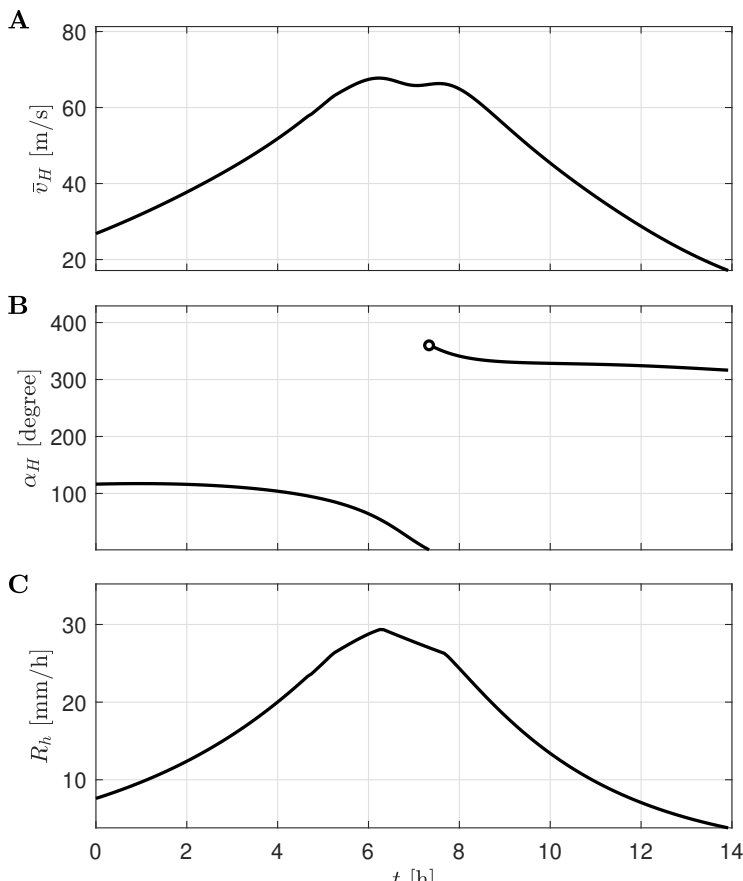


Figure 4. The simulated category V hurricane in Saffir-Simpson scale measured at the building site: (A) evolution of the mean hourly wind speed; (B) wind direction; and (C) mean hourly rainfall intensity.

time evolution of mean hourly wind speed $\bar{v}_H(t)$, wind direction $\alpha_H(t)$ (measured counterclockwise from south), and mean hourly rainfall intensity $R_h(t)$ are reported in **Figure 4**. An example of the corresponding non-stationary/-straight/-Gaussian wind pressure simulated through the procedure of Sec. 4.1 is shown in **Figure 5** for an envelope component located at the upper-left corner of the front face of the building.

Figure 6 reports the accumulation of damage over the duration of the hurricane in terms of the total number of envelope components assuming DS_{Dr_1} , DS_{Dr_2} or $DS_{P_{60}}$. From the comparison between the damage histories and the wind speed history of **Figure 4A**, it can be seen that most damage occurs near the time of the maximum wind speed time, i.e. during the 7th hour of the hurricane event. By the end of the hurricane event, the final damage states for each envelope component was recorded, and are reported in **Table 2** in terms of the number of damaged components on each face of the building. As can been seen, due to the continually varying wind direction, the damage is relatively evenly distributed between the faces. The distribution of final damages shows how pressure-induced damages are dominant, which is consistent with the results reported in (Ouyang and Spence, 2020) for a nominal hurricane representation. Water ingress is also recorded during and at the end of the hurricane, where a total volume of 270.5 m³ of water was estimated to enter the building through the damaged envelope components. The time histories of water ingress at each floor during the hurricane are reported in **Figure 7** and shows how water ingress towards the bottom of the building dominates.

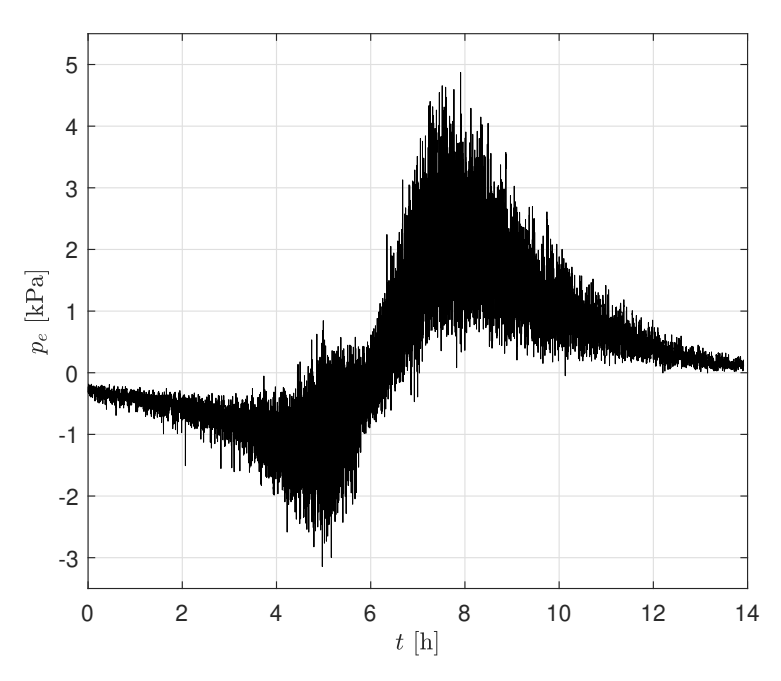


Figure 5. An example of the non-stationary/-straight/-Gaussian external wind pressure process for an envelope component located at the upper-left corner of the front face of the building.

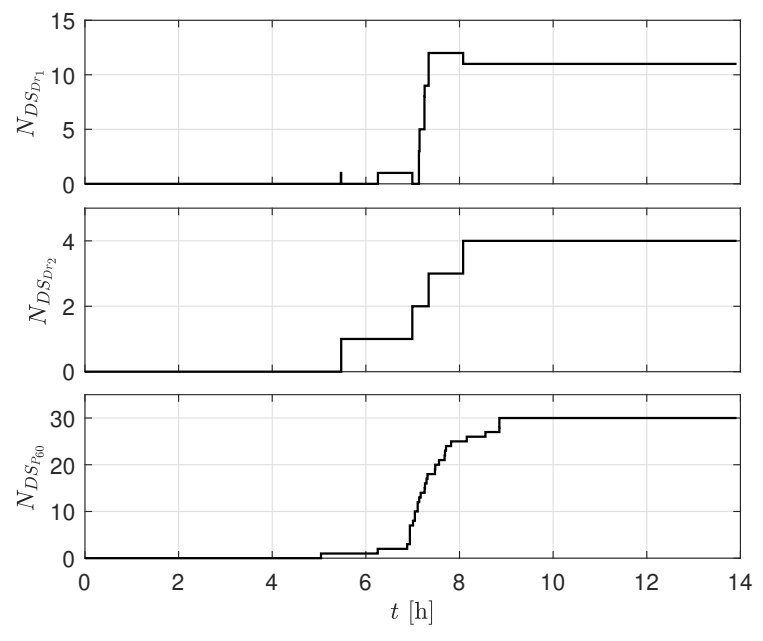


Figure 6. Time histories of the total number of components in damage states DS_{Dr_1} , DS_{Dr_2} and $DS_{P_{60}}$.

8.3.3 Probabilistic performance metrics

516

517

518

519

520

521

522

The mean annual rate of each envelope component assuming as a final damage state DS_{Dr_1} , DS_{Dr_2} , or $DS_{P_{60}}$ are reported in **Figure 8**. The damage maps show how the drift-induced damages are uniformly distributed over the envelope except for the top and bottom floors, while the pressure-induced damages are more concentrated near the edges of the building due to the local aerodynamic response of the system. Overall, the damage patterns and rates are similar to those seen for the nominal hurricane setting analyzed in (Ouyang and Spence, 2020).

Table 2. Number of envelope components assuming DS_{Dr_1} , DS_{Dr_2} or $DS_{P_{60}}$ as final damage state.

Final damage state	South face	East face	North face	West face
DS_{Dr_1}	4	3	1	3
DS_{Dr_2}	0	2	1	1
$DS_{P_{60}}^{-12}$	5	12	4	11

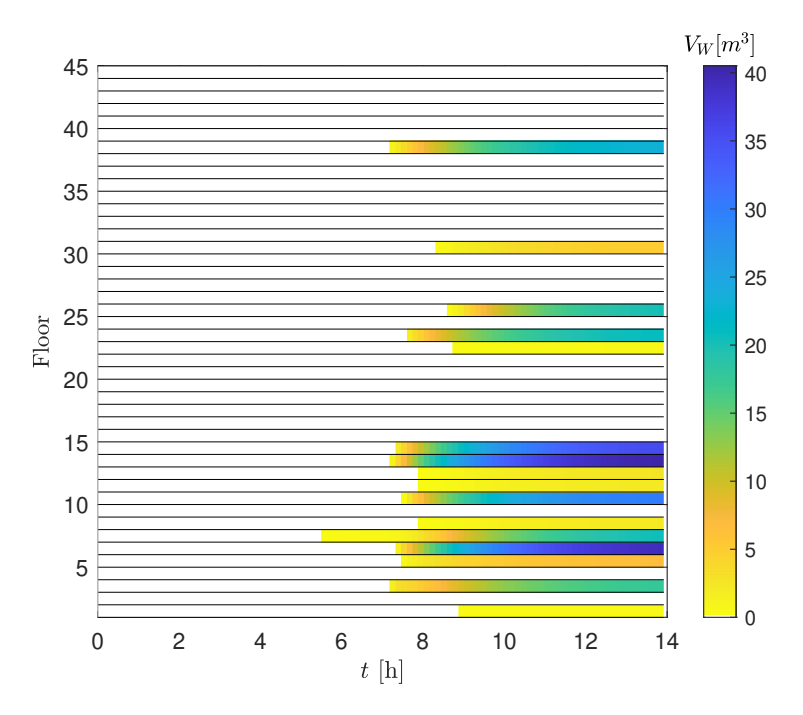


Figure 7. Time histories of the water ingress at each floor.

To evaluate the system-level envelope performance for both the nominal and full hurricanes, **Figure 9** reports the damage curves for both scenarios in terms of the mean annual rate of exceeding a total number of components assuming as a final damage state DS_{Dr_1} , DS_{Dr_2} , or $DS_{P_{60}}$. Comparison between the drift induced damage curves show how the total number of damaged components are well estimated by the nominal hurricane for annual rates greater than 2×10^{-6} . However, for rarer events, the nominal hurricane will generally lead to considerable overestimation of damage. For pressure-induced damage, it can be seen that the nominal hurricanes underestimate the damages for mean annual rates greater than 2×10^{-6} , but once again significantly overestimate damages for rarer events. The differences in **Figure 9** are likely caused by the duration of the maximum wind T_m , where T_m is defined as the duration when the hurricane wind speed $\bar{v}_H(t)$ is within a certain percentage of the maximum wind speed $\hat{v}_H = \max[\bar{v}_H(t)]$ (e.g., $\bar{v}_H(t) \geq 0.95\hat{v}_H$). Indeed, the storm track model considered in this study suggests that hurricanes with a larger maximum mean wind speed, \hat{v}_H , have a relatively "sharper" wind speed history curve (i.e. the duration of the maximum wind is shorter).

To investigate this, the distribution of maximum wind speed duration is analyzed for all hurricane samples in hazard intervals three to nine, where the first two intervals are not considered as the value of \hat{v}_H is negligible from an engineering standpoint. The mean and standard deviation of the duration are reported in **Figure 10**, from which it can be seen that as the hurricane event becomes rarer, the duration of maximum wind becomes shorter. In particular, it can be seen that wind speeds within 98% of the maximum have an expected duration of around 1-hour. The capability of the nominal hurricane in adequately reproducing

the damage would suggest that envelope damage is occurring essentially when wind speeds are at their maximum.

The loss curves associated with repair costs are reported in **Figure 11**. The relative magnitude of total repair cost between the nominal and full hurricanes are similar to the damage curves of **Figure 9C**, which implies that the pressure-induced damages dominate the total repair cost associated with the envelope components. **Figure 12** reports the exceedance rates associated with the consequence metric of total volume of water ingress V_W . From the comparison of the water ingress curves, the nominal hurricane significantly underestimates the total amount of water ingress as compared to the full hurricane. To quantify this underestimation, **Table 3** reports the total water ingress at different exceedance rates for the nominal and full hurricanes. As can be seen, a near 40 fold underestimation of water ingress can be seen for exceedance rates of 1×10^{-3} . The root of this difference can be traced back to how the nominal hurricane neglects the water that can enter the building due to rainfall after the peak wind speeds have occurred. As the exceedance rates decrease, the underestimation of total water ingress from the nominal hurricane also decreases. This is due to how as the hurricane events become more extreme, the majority of damage will occur at the beginning of the nominal hurricane event therefore increasing the duration in which water can ingress.

Table 3. Comparison between total water ingress in the nominal hurricane $(V_W^{(n)})$ and full hurricane $(V_W^{(f)})$.

Mean annual rate	$V_W^{(n)}$ (m ³)	$V_W^{(f)}$ (m ³)	$V_W^{(n)}/V_W^{(f)}$
$\lambda = 1 \times 10^{-3}$	1.68	63.10	37.56
$\lambda = 1 \times 10^{-4}$	46.49	867.17	18.65
$\lambda = 1 \times 10^{-5}$	316.40	2549.87	8.06
$\lambda = 1 \times 10^{-6}$	925.18	6268.17	6.78

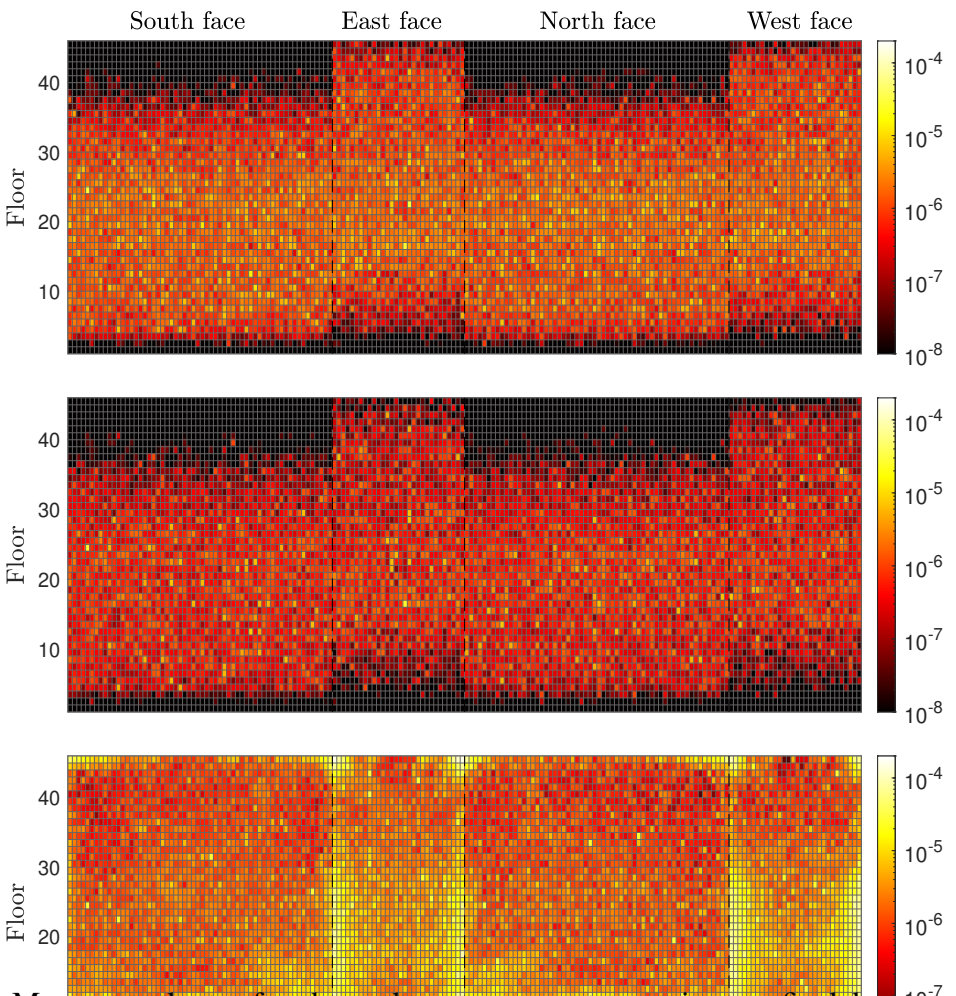


Figure 8. Mean annual rate of each envelope component assuming as a final damage state DS_{Dr_1} , DS_{Dr_2} , or $DS_{P_{60}}$. Top panel is associated with DS_{Dr_1} , middle panel with DS_{Dr_2} , and pottom panel with $DS_{P_{60}}$.

9 SUMMARY AND CONCLUSION

A framework is outlined for the performance assessment of the envelope system of engineered buildings subject to a full representation of the hurricane hazard. A new wind-tunnel informed POD-based non-stationary/-straight/-Gaussian wind pressure stochastic simulation model is introduced to support the full hurricane event simulation. Through the development of a conditional stochastic simulation framework, efficient estimation of probabilistic metrics associated with the performance of the envelope system in rare events is made possible. The framework was illustrated through a case study consisting in a 45-story archetype building located in Miami, FL. Performance metrics associated with the total number of damaged envelope components, monetary loss, and total water ingress were evaluated. The comparison of the performance metrics with those estimated for a classic nominal representation of the hurricane hazard showed that performance assessments made with the nominal hurricane representation will generate similar amounts of damages and losses for mean annual rate greater than 2×10^{-6} . For events with smaller rates than 2×10^{-6} , the nominal hurricanes significantly overestimated (up to 50%) the damages and losses. In terms of the water ingress, a full hurricane representation will generate a much larger volume of water

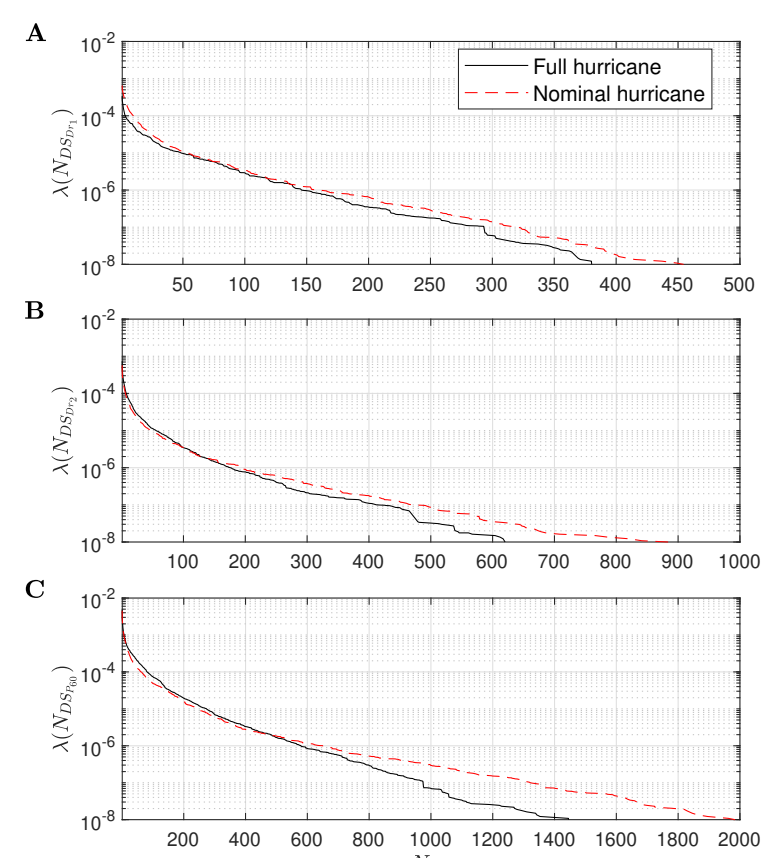


Figure 9. Mean annual rate of exceeding a total number of envelope components assuming as a final damage state: (A) DS_{Dr_1} ; (B) DS_{Dr_2} ; (C) $DS_{P_{60}}$.

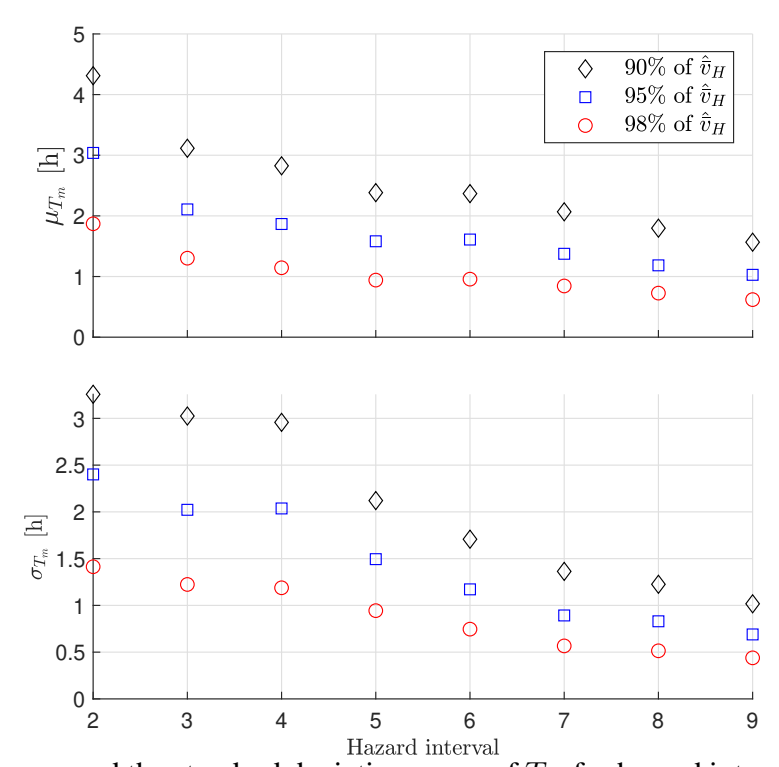


Figure 10. Mean, μ_{T_m} , and the standard deviation, σ_{T_m} , of T_m for hazard intensity intervals three to nine.

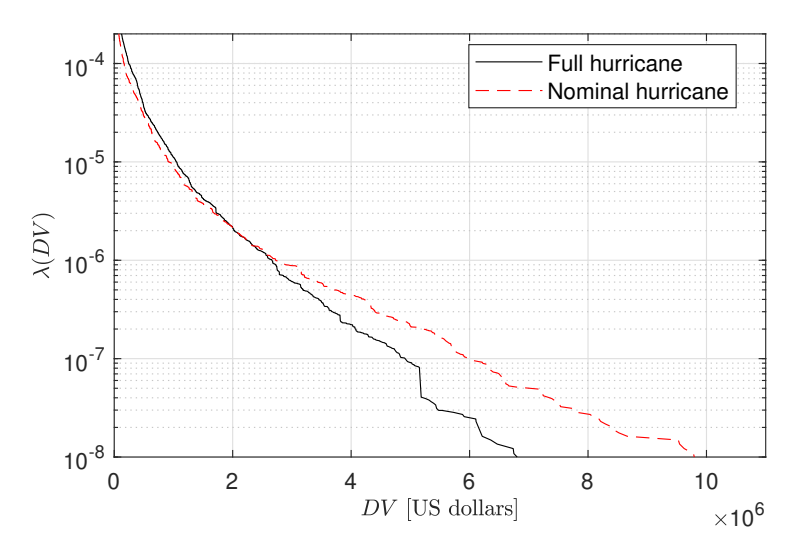


Figure 11. Repair cost loss curves in US dollars for the nominal and full hurricanes.

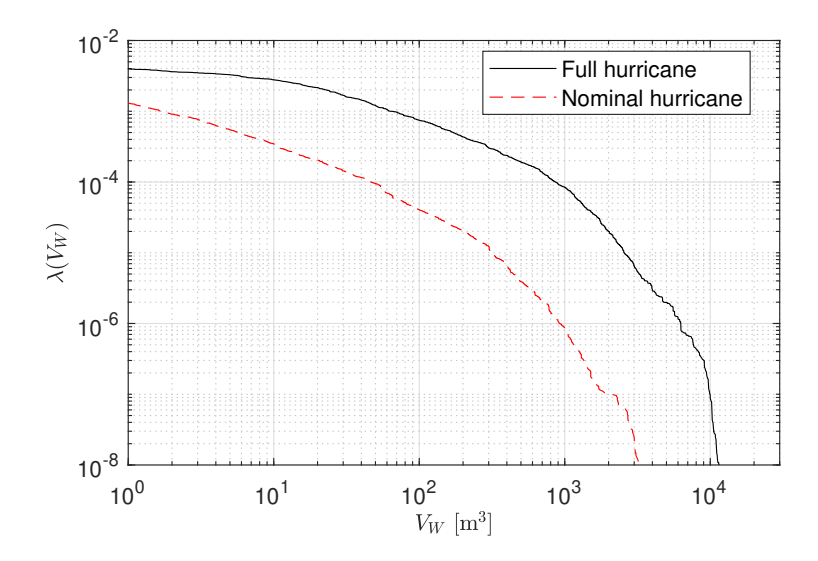


Figure 12. Consequence curve associated with total water ingress due to envelope damage.

ingress, over 30 fold larger for rates of 1×10^{-3} , than seen for simulations using a nominal hurricane representation. This underestimation was seen to decrease with the reduction of the exceedance rates.

CONFLICT OF INTEREST STATEMENT

The authors declare that the research was conducted in the absence of any commercial or financial relationships that could be construed as a potential conflict of interest.

AUTHOR CONTRIBUTIONS

All authors listed have made a substantial, direct, and intellectual contribution to the work and approved it for publication.

FUNDING

- 576 The research effort was supported in part by the United States (US) National Science Foundation (NSF)
- 577 under Grants No. CMMI-1562388 and CMMI-1750339. This support is gratefully acknowledged.

DATA AVAILABILITY STATEMENT

- The original contributions presented in the study are included in the article/supplementary material, further
- 579 inquiries can be directed to the corresponding author/s.

REFERENCES

- 580 Au, S. K. and Beck, J. L. (2001). Estimation of small failure probabilities in high dimensions by subset
- simulation. *Probabilistic engineering mechanics* 16, 263–277
- 582 Barbato, M., Petrini, F., Unnikrishnan, V. U., and Ciampoli, M. (2013). Performance-based hurricane
- engineering (PBHE) framework. *Structural Safety* 45, 24–35
- 584 Bernardini, E., Spence, S. M. J., Kwon, D.-K., and Kareem, A. (2015). Performance-based design of
- 585 high-rise buildings for occupant comfort. Journal of Structural Engineering 141
- 586 Brackins, J. T. and Kalyanapu, A. J. (2020). Evaluation of parametric precipitation models in reproducing
- tropical cyclone rainfall patterns. *Journal of Hydrology* 580, 124255
- 588 Chen, S. S., Knaff, J. A., and Marks, F. D. (2006). Effects of vertical wind shear and storm motionon
- tropical cyclone rainfall asymmetries deduced from TRMM. *Monthly Weather Review* 134, 3190–3208
- 590 Chuang, W. and Spence, S. M. J. (2017). A performance-based design framework for the integrated
- collapse and non-collapse assessment of wind excited buildings. *Engineering Structures* 150, 746–758
- 592 Ciampoli, M., Petrini, F., and Augusti, G. (2011). Performance-based wind engineering: Towards a
- 593 general procedure. *Structural Safety* 33, 367–378
- 594 Cui, W. and Caracoglia, L. (2018). A unified framework for performance-based wind engineering of tall
- buildings in hurricane-prone regions based on lifetime intervention-cost estimation. Structural Safety
- 596 73, 75–86
- 597 Cui, W. and Caracoglia, L. (2020). Performance-based wind engineering of tall buildings examining
- 598 life-cycle downtime and multisource wind damage. Journal of Structural Engineering 146
- 599 Cui, W., Zhao, L., Cao, S., and Ge, Y. (2021). Bayesian optimization of typhoon full-track simulation
- on the northwestern pacific segmented by quadtree decomposition. *Journal of Wind Engineering and*
- 601 Industrial Aerodynamics 208, 104428
- 602 Federal Emergency Management Agency (FEMA) (2012b). Seismic Performance Assessment of
- 603 Buildings, Volume 1 Methodology (FEMA Publication P-58-2). Tech. rep., Washington, D.C.
- 604 Geoghegan, K. M., Fitzpatrick, P., Kolar, R. L., and Dresback, K. M. (2018). Evaluation of a synthetic
- rainfall model, p-cliper, for use in coastal flood modeling. *Natural Hazards* 92, 699–726
- 606 Grieser, J. and Jewson, S. (2012). The rms tc-rain model. Meteorologische Zeitschrift 21, 79
- 607 Guha, T. K., Sharma, R. N., and Richards, P. J. (2011). Internal pressure dynamics of a leaky building
- with a dominant opening. Journal of Wind Engineering and Industrial Aerodynamics 99, 1151–1161
- Huang, S. H. and Li, Q. S. (2012). Large eddy simulations of wind-driven rain on tall building facades.
 Journal of Structural Engineering 138, 967–983
- 611 Ierimonti, L., Venanzi, I., Caracoglia, L., and Materazzi, A. L. (2019). Cost-based design of nonstructural
- elements for tall buildings under extreme wind environments. Journal of Aerospace Engineering 32,
- 613 04019020

- Jakobsen, F. and Madsen, H. (2004). Comparison and further development of parametric tropical cyclone
- 615 models for storm surge modelling. Journal of Wind Engineering and Industrial Aerodynamics 92,
- 616 375–391
- 617 Kubilay, A., Derome, D., Blocken, B., and Carmeliet, J. (2013). CFD simulation and validation of wind-
- driven rain on a building facade with an Eulerian multiphase model. Building and Environment 61, 69
- 619 -81
- 620 Kubilay, A., Derome, D., Blocken, B., and Carmeliet, J. (2015). Numerical modeling of turbulent
- dispersion for wind-driven rain on building facades. *Environmental Fluid Mechanics* 15, 109–133
- 622 Kubilay, A., Derome, D., and Carmeliet, J. (2017). Analysis of time-resolved wind-driven rain on an array
- of low-rise cubic buildings using large eddy simulation and an eulerian multiphase model. *Building and*
- 624 Environment 114, 68–81
- 625 Lonfat, M., Marks, F. D., and Chen, S. (2004). Precipitation distribution in tropical cyclones using
- the tropical rainfall measuring mission (TRMM) microwave imager: A global perspective. *Monthly*
- 627 *Weather Review* 132, 1645–1660
- 628 Lonfat, M., Rogers, R., Marchok, T., and Marks Jr, F. D. (2007). A parametric model for predicting
- 629 hurricane rainfall. *Monthly Weather Review* 135, 3086–3097
- 630 Micheli, L., Alipour, A., Laflamme, S., and Sarkar, P. (2019). Performance-based design with life-cycle
- cost assessment for damping systems integrated in wind excited tall buildings. *Engineering Structures*
- 632 195, 438–451
- 633 Ouyang, Z. and Spence, S. M. J. (2019). A performance-based damage estimation framework for the
- 634 building envelope of wind-excited engineered structures. Journal of Wind Engineering and Industrial
- 635 *Aerodynamics* 186, 139–154
- 636 Ouyang, Z. and Spence, S. M. J. (2020). A performance-based wind engineering framework for envelope
- 637 systems of engineered buildings subject to directional wind and rain hazards. Journal of Structural
- 638 Engineering 146, 04020049
- 639 Ouyang, Z. and Spence, S. M. J. (2021). Performance-based wind-induced structural and envelope
- damage assessment of engineered buildings through nonlinear dynamic analysis. Journal of Wind
- Engineering and Industrial Aerodynamics 208, 104452
- 642 Petrini, F. and Ciampoli, M. (2012). Performance-based wind design of tall buildings. Structure and
- 643 Infrastructure Engineering 8, 954–966
- 644 Pita, G., Pinelli, J. P., Gurley, K., Subramanian, C., and Hamid, S. (2016). Hurricane vulnerability model
- for mid/high-rise residential buildings. *Wind and Structures* 23, 449–464
- Porter, K. A. (2003). An Overview of PEER's Performance-Based Earthquake Engineering Methodology.
- 647 Proc. Ninth International Conference on Applications of Statistics and Probability in Civil Engineering
- 648 (*ICASP9*)
- 649 Smith, M. A. and Caracoglia, L. (2011). A Monte Carlo based method for the dynamic "fragility analysis"
- of tall buildings under turbulent wind loading. *Engineering Structures* 33, 410–420
- 651 Snaiki, R. and Wu, T. (2018). An analytical framework for rapid estimate of rain rate during tropical
- 652 cyclones. Journal of Wind Engineering and Industrial Aerodynamics 174, 50–60
- 653 Taylor, H. T., Ward, B., Willis, M., and Zaleski, W. (2010). The saffir-simpson hurricane wind scale.
- 654 Atmospheric Administration: Washington, DC, USA
- 655 [Dataset] Tokyo Polytechnic University (2008). TPU Wind Pressure Database
- 656 Vickery, B. J. and Bloxham, C. (1992). Internal pressure dynamics with a dominant opening. *Journal of*
- 657 Wind Engineering and Industrial Aerodynamics 41, 193–204

- Vickery, P. J., Skerlj, P., Steckley, A. C., and Twisdale, L. A. (2000a). Hurricane wind field model for use in hurricane simulations. *Journal of Structural Engineering* 126, 1203–1221
- Vickery, P. J., Skerlj, P. F., and Twisdale, L. A. (2000b). Simulation of hurricane risk in the us using empirical track model. *Journal of structural engineering* 126, 1222–1237
- Vickery, P. J. and Twisdale, L. A. (1995a). Prediction of hurricane wind speeds in the united states.
 Journal of Structural Engineering 121, 1691–1699
- Vickery, P. J. and Twisdale, L. A. (1995b). Wind-field and filling models for hurricane wind-speed predictions. *Journal of Structural Engineering* 121, 1700–1709
- Yu, S., Lou, W., and Sun, B. (2008). Wind-induced internal pressure response for structure with single windward opening and background leakage. *Journal of Zhejiang University-SCIENCE A* 9, 313–321

APPENDIX

668 Structural system

The layout of the structural system is shown in Figure 2 with beams and columns grouped in plan as 669 shown in Figure 2B. Groups of beams and columns extend three consecutive floors. The diagonal braces 670 are grouped as pairs over the height of the building. The beams and bracing elements are assigned sections 671 from the W24 AISC (American Institute for Steel Construction) family while the columns are box sections 672 with wall thickness taken as 1/20 of the mid-line width of the section. The floors are considered rigid in 673 their plane with a mass density of 0.38 t/m². The damping ratio for each vibration mode was taken as 674 a lognormal random variable of mean 0.014 and coefficient of variation 0.3. The structural system was 675 designed to meet: 1) 1/400 story drift ratios under 50-year mean recurrence interval (MRI) wind blowing 676 down the x or y directions; and 2) demand to capacity ratios of less than one for 1700-year MRI wind 677 blowing down the x or y directions. The resulting member sizes are reported in **Table 4**. 678

679 Envelop system

683

690

Each glass panel was mounted 0.5 m from the upper floor and 1.5 m from the lower floor. The cladding system was considered not to provide lateral stiffness. The equivalent net pressure demand was defined as:

$$p_{eq}(t;\xi_{xyz}) = \left(\frac{1}{t_{eq}} \int_0^t [p_n(t;\xi_{xyz})]^s\right)^{\frac{1}{s}}$$
(33)

damage model of Sec. 5.2.1, the occurrence of DS_{Dr_1} or DS_{Dr_2} was considered to result in an reduction in capacity to resist p_{eq} of 10% and 80% respectively. To account for uncertainty, the reductions were taken as the means of truncated normal distributions of support [0,1] and coefficient of variation of 0.1. All damage states were considered to require the replacement of the glazing unit. In calibrating the model of Sec. 6, a single consequence function was therefore required. The median values of the consequence function were: $Q_{\min} = 20$, $Q_{\max} = 100$, $Q_{\max} = 2955$ [USD], and $Q_{\min} = 1576$ [USD]. Uncertainty was

with $t_{eq}=60~{\rm s}$ and s=16. The damage state DSP_{60} was considered terminal. In calibrating the coupled

modeled through assigning a log-normal distribution of dispersion of 0.1185 to the consequence function.

- 691 Wind-driven rain simulation
- The normalized specific catch ratios necessary for calibrating the interpolation-based scheme of Sec. 4.2 were estimated in OpenFOAM 4.1. Three computational domains were considered for wind angles of $\alpha_H = 0^{\circ}$, $\alpha_H = 45^{\circ}$ and $\alpha_H = 90^{\circ}$. Each domain extended, at full scale, 900 m upwind/laterally and

695

696

697

698

699

700

Table 4. Member sizes for for the structural system. D1 indicate diagonals while W24 sections are identified through their weight per unit length using imperial units. Box sections are identified in terms of their

mid-line width in cm.

Group	Floor Number														
Number	1-3	4-6	7-9	10-12	13-15	16-18	19-21	22-24	25-27	28-30	31-33	34-36	37-39	40-42	43-45
B1	146	146	146	146	162	162	146	162	131	131	131	131	131	131	131
B2	162	370	370	370	370	370	370	306	306	250	192	192	162	192	192
В3	450	408	492	492	450	450	450	450	492	450	450	408	250	207	192
B4	335	408	408	408	450	450	450	408	370	370	306	279	229	192	176
B5	176	250	250	229	192	176	176	176	162	162	162	162	146	146	146
В6	335	335	306	306	279	279	250	250	279	229	207	192	192	162	162
D1	335	306	279	250	250	279	370	492	492	492	492	370	279	162	192
C1	55	50	50	50	50	50	45	45	45	45	45	45	45	45	45
C2	55	50	50	50	50	50	45	45	45	45	45	45	45	45	50
C3	55	50	50	50	55	50	50	50	45	50	50	45	50	50	50
C4	60	55	50	60	55	55	50	50	50	50	50	50	50	50	50
C5	60	55	55	60	60	55	55	55	55	55	55	50	55	50	55
C6	70	70	70	65	65	65	65	60	60	60	60	55	55	55	55
C7	80	80	80	80	80	75	75	70	70	70	65	65	60	60	60
C8	175	125	105	105	90	90	85	75	75	70	65	65	60	60	55
C9	85	90	90	85	85	85	85	85	80	80	75	75	70	60	55
C10	90	85	85	90	85	80	80	80	85	80	80	75	70	65	55
C11	110	80	75	80	80	75	75	75	75	70	70	70	65	65	55
C12	55	75	75	75	75	75	70	70	70	65	60	55	60	55	50
C13	65	70	70	70	75	75	75	70	70	65	65	65	60	60	60
C14	65	65	60	60	55	55	50	50	50	50	50	50	50	45	45
C15	65	60	60	60	55	55	55	55	55	50	50	50	50	50	50
C16	160	100	90	80	70	65	60	55	55	55	50	50	50	50	50
C17	80	80	80	75	70	65	60	55	55	60	55	55	50	50	45
C18	70	75	70	65	65	65	65	65	65	65	65	60	60	55	55

2700 m downwind of the building. Each domain had a total of 139500 rectangular elements in a structured mesh. Seventeen rain phases were considered with raindrop diameters ranging from 0.3 mm to 2.4 mm with a 0.3 mm increment and from 2.4 mm to 6 mm with an increment of 0.4 mm. Through symmetry, the simulation results were extended to wind directions of 135° , 180° , 225° , 270° and 315° . Solutions were estimated for the wind speeds defining the boundaries of the 9 conditional failure events used in deriving the hazard curve of Sec. 8.2.